Ain Shams Engineering Journal 14 (2023) 102037

Contents lists available at ScienceDirect

Ain Shams Engineering Journal

journal homepage: www.sciencedirect.com

An improved predictive current control for IM drives

Fahimeh Shiravani [a,*], Patxi Alkorta [a], Jose Antonio Cortajarena [b], Oscar Barambones [c]

[a] Department of Systems Engineering and Automation, University of the Basque Country (UPV/EHU) Engineering School of Gipuzkoa, Eibar section, Otaola hiribidea 29, 20600 Eibar, Spain
[b] Department of Electronic Technology, University of the Basque Country (UPV/EHU) Engineering School of Gipuzkoa, Eibar section, Otaola hiribidea 29, 20600 Eibar, Spain
[c] Department of Systems Engineering and Automation, University of the Basque Country (UPV/EHU) Engineering school of Vitoria, Avenida Nieves Cano 12, 01006 Vitoria, Alava, Spain

ARTICLE INFO

Article history:
Received 23 July 2022
Revised 28 September 2022
Accepted 30 October 2022
Available online 18 November 2022

Keywords:
Induction motor
Predictive current control
Voltage vector
VSI
Experimental validation

ABSTRACT

In Finite Control Set-Model Predictive Control (FCS-MPC), the model of the induction machine (IM) is expressed in the $\alpha - \beta$ or $d - q$ reference frame, and then the back-EMF is estimated based on the applied voltage vectors. In this work, the d-q reference frame is used but unlike the existing method, the estimated back-EMF is calculated by filtering the voltage vectors. Moreover, the work studies the importance of the discretization method on the predictive control behavior of IM. It has been demonstrated that the mentioned enhancements lead to an efficient Total Harmonic Distortion value for stator current (THD_i) and torque ripple reduction compared to the conventional methods. The proposed Predictive Current Controller (PCC) has been validated experimentally by using a commercial IM of 7.5[kW] controlled by a dSpace 1103 real-time control board running with sample frequencies from 10[kHz]to 80[kHz]. The test results validate the developed controller's ability to meet the control objectives in a whole range of speeds, loads, and sampling frequencies.

1. Introduction

Model predictive control (MPC) was the first introduced in the late 1970s and has evolved considerably since then. In the last three decades, it has experienced a major breakthrough in the control research community and in industry. MPC is undoubtedly the most general technique for expressing the process control problem in the time domain, which explains its success [1]. However, compared to traditional control systems, these type of controllers have a large computational burden. Therefore, predictive algorithms were first used in slow dynamics applications. Due to technical advances in microprocessors, especially in digital signal processing (DSP), the predictive technique started to be applied in processes with a fast dynamic response. Predictive control is being used in a variety of applications with great success. Wind turbine systems [2,3], drying towers [4], power systems [5–7], servos [8], and robotic arms [9] can be named as some of the applications of this method.

The regulation of alternating current (AC) in power systems and its total harmonic distortion (THD_i) is one of the most classic and challenging topics in electrical engineering [10]. The THD_i is a key aspect to consider in power systems, and must be kept to a minimum. In a power system, a lower THD_i means a higher power factor [11], lower peak currents and related power losses and, as a result, higher efficiency. A low THD_i is so important in power systems that international standards such as $IEC61000-3-2$ and $IEEE519$ specify harmonic current restrictions for different classes of power equipment. In the literature, several control systems have been developed to manage the AC of electric drives [12–14]. In several cases, conventional PI-based controllers have been employed with the PWM approach. On the other hand, the PI technique requires parameter tuning, which is often carried out through a series of trial-and-error processes, and requires re-tuning if the system undergoes changes, i.e., such as machine replacement. External PWM modules should be used in combination with PI controllers as well [15].

Predictive control has a variety of characteristics that make it ideal for power converter control: the principles are clear and easy to comprehend; they can be applied to a wide range of systems; constraints and nonlinearities can be easily integrated; the multivariable case can be addressed; and the final controller is simple to create [16]. However, while MPC for power converters and drives is a well-known research and development approach, further

* Corresponding author.
E-mail address: fahimeh.shiravani@ehu.eus (F. Shiravani).

Peer review under responsibility of Ain Shams University.

Production and hosting by Elsevier

https://doi.org/10.1016/j.asej.2022.102037
2090-4479/

research and development is necessary to get this technology to a commercial and industrial level [17].

The continuous control set MPC (CCS-MPC) [18,19] and the finite control set MPC (FCS-MPC) [20,21] are two of the most common MPC variants in power electronics. The output of the CCS-MPC is a voltage vector that is obtained by solving an online optimization problem and then must pass through the PWM modulation module [22]. In the FCS-MPC, however, the inherent discrete characteristic of the inverter and a load model is used to solve the optimization problem [23]. There are two types of FCS-MPC used in power electronics: finite control set Predictive Torque Control (PTC) [24] and finite control set Predictive Current Control (PCC) [25,26]. The main objective of both finite control set techniques is to use a predictive torque/current controller to replace the inner PI current regulators and PWM block set, resulting in faster dynamics.

PTC and PCC are model-based methods indicating that having an accurate approximation of the model leads to better control in these strategies. In addition, because digital control systems work with discrete or digital signals, the drive model must be discretized. The Forward Euler approximation, for example, is a relatively simple and commonly used method for discretizing the continuous-time model of the electrical load in a finite set of control-based approaches [16,27]. Unfortunately, at high frequencies the Euler approximation produces significant modeling error, which presents problems when large bandwidths are handled [28]. In [29] the accuracy of the IM model by using different discretization methods for MPC is investigated. Then, in [30,31] is studied the impact of a better discretization method on the performance of the PMSM while MPC is applied.

To address the aforementioned issue, this research provides a control system for IM based on a PCC finite control set. The proposed solution eliminates the need of inner PI current controllers and PWM block. Faster control with acceptable steady-state and dynamic performance is enabled by the FCS-MPC, which anticipates future states of the control objectives and corrects errors before applying switching signals to the inverter. The following are the major contributions of this work:

- Electric load model is discretized by using the Taylor series expansion. As a result, a simple and discrete-time description of the load model is obtained, which is more accurate than the simple Euler model and guarantees a trade-off between model accuracy and complexity.
- The design has been done in the rotating reference frame $d-q$ to facilitate the use of a Low Pass Filter (LPF) to enhance the estimated back-EMF. It is demonstrated that this change has a remarkable impact on THD_i reduction and torque ripple minimization.
- Both in simulation and experimental tests, the proposed method is validated for a wide range of speed, load torque, and sampling frequency. Also, it is worth to be mentioned that this proposal does not imply a high computational cost.

This paper is organized as follows: Section 2 briefly reviews the two-level voltage inverter model and IM system. The structure of the proposed PCC is explained in Section 3. The effectiveness of the proposed controller is obtained by numerical simulation and experimental prototype, and they are presented in Section 4. Finally, the conclusion has been discussed in Section 5.

2. Drive Model

An induction motor is connected to the output of the three-phase two-level Voltage Source Inverter (VSI), and the V_{DC} voltage source is provided for Direct Current (DC) link (Fig. 1(a)).

The gating signals determine the switching binary states of the converter S_A, S_B, and S_C. To avoid short-circuiting the DC source, one limitation for the proper operation of this converter is that the two switches in each leg must work in a complementary mode.

According to a combination of switching binary states, the three-phase VSI with six switches has a total of eight voltage vectors: $2^3 = 8$. Only six voltage vectors are considered active as control elements since the other two vectors are null, Fig. 1(b). The output voltage space vectors are based on the state of inverter switches. As,

$$\vec{S} = \frac{2}{3}\left(S_A + e^{\frac{j2\Pi}{3}}S_B + e^{\frac{j4\Pi}{3}}S_C\right) \tag{1}$$

the output voltage vector is as follow,

$$\vec{v}_{\alpha,\beta} = V_{DC}.\vec{S} \tag{2}$$

where V_{DC} is the DC link voltage and $\vec{v}_{\alpha,\beta}$ is the voltage vector that inverter generates. The output current vector can be expressed as,

$$\vec{i} = \frac{2}{3}(i_A + e^{\frac{j2\Pi}{3}}i_B + e^{\frac{j2\Pi}{3}}i_C) \tag{3}$$

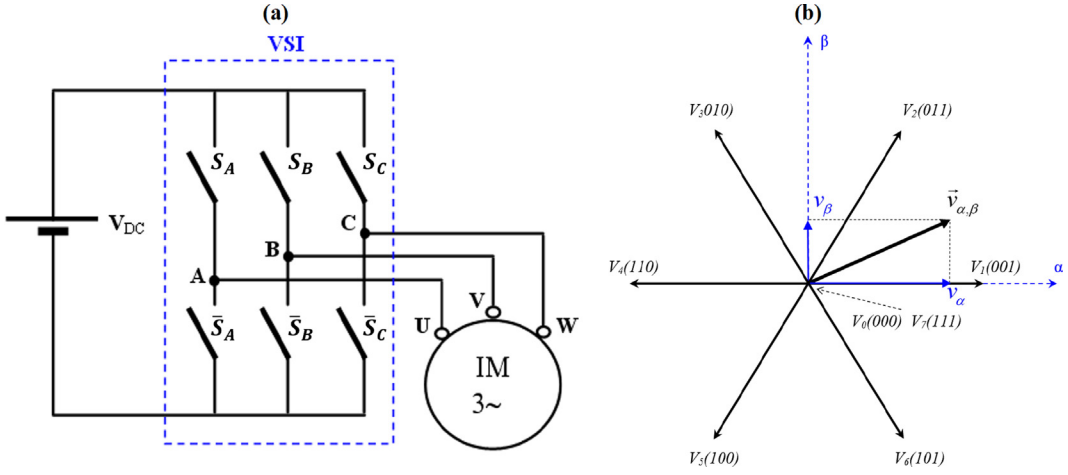

Fig. 1. (a) Two-level VSI. (b) The 8 voltage vectors generated by two-level VSI inverter.

where i_A, i_B and i_C are the three phase output currents. Having from [16] the idea to employ the PCC algorithm with the general three-phase load current dynamics,

$$\vec{v}_{\alpha,\beta} = L\frac{d\vec{i}_{\alpha,\beta}}{dt} + R\vec{i}_{\alpha,\beta} + \vec{e}_{\alpha,\beta} \tag{4}$$

and applying to the three-phase stator of squirrel cage IM, it is obtained,

$$\vec{v}_{\alpha,\beta} = \sigma L_s\frac{d\vec{i}_{\alpha,\beta}}{dt} + R_s\vec{i}_{\alpha,\beta} + \vec{e}_{\alpha,\beta} \tag{5}$$

where σ, L_s, and R_s stand for the coefficient of magnetic dispersion, stator inductance, and stator resistance, respectively. Also, $\vec{e}_{\alpha,\beta}$ represents the load back-EMF vector.

The main idea of the PCC algorithm is to predict the optimal $\vec{v}_{\alpha,\beta}$ voltage vector that the VSI generates to get the best stator current control in each sample period. This is obtained by minimizing a cost function related to the stator's current errors. These currents can be expressed in the $\alpha-\beta$ stationary reference frame, [16], or to get the best results and as in this paper is proposed, taking them in the $d-q$ rotating reference frame. Considering this explanation, the following cost function is proposed based on $\vec{i}_{d,q}$,

$$g = \left|i_d^*(k+1) - i_d(k+1)\right|^2 + \left|i_q^*(k+1) - i_q(k+1)\right|^2 \tag{6}$$

where $\vec{i}_d^*(k+1)$ is the future d current component reference, given by the rotor flux loop reference and $\vec{i}_q^*(k+1)$ is the future q current component reference given by the speed loop regulator. When these references are not obtained from the predictive type controllers, like in this case, then can be considered $\vec{i}_{d,q}^*(k+1) \approx \vec{i}_{d,q}^*(k)$ [16]. Regarding the two current components predictions, $\vec{i}_{d,q}(k+1)$, the formulation of the three-phase stator voltage in $d-q$ rotating reference frame is taken as,

$$\vec{v}_{d,q} = \sigma L_s\frac{d\vec{i}_{d,q}}{dt} + R_s\vec{i}_{d,q} + \vec{e}_{d,q} \tag{7}$$

Also, considering the discrete nature of the digital control platforms, Eq. (7) has to be discretized for both current components. Therefore, considering, and then, taking the Euler discretization method leads to,

$$\vec{i}_{d,q}(k) = \frac{1}{R_sT_s+\sigma L_s}[\sigma L_s\vec{i}_{d,q}(k-1) + \vec{v}_{d,q}(k)T_s - \vec{e}_{d,q}(k)T] \tag{8}$$

and project it to a sample period ahead, the two current components predictions that are needed for Eq. (6) are being obtained as,

$$\vec{i}_{d,q}(k+1) = \frac{1}{R_sT_s+\sigma L_s}[\sigma L_s\vec{i}_{d,q}(k) + \vec{v}_{d,q}(k+1)T_s - \vec{e}_{d,q}(k+1)T] \tag{9}$$

Now we can consider that $\vec{e}_{d,q}(k+1) \approx \vec{e}_{d,q}(k)$. Hence, the back-EMF can be estimated by using Eq. (7) and discretized by Euler method, as,

$$\hat{\vec{e}}_{d,q}(k) = \vec{v}_{d,q-fil}(k) + \frac{L_s}{T_s}\vec{i}_{d,q}(k-1) - \frac{R_sT_s+\sigma L_s}{T_s}\vec{i}_{d,q}(k) \tag{10}$$

In back-EMF estimation (10), the value of $\vec{v}_{d,q-fil}(k)$ is obtained by applying a LPF to $\vec{v}_{d,q}(k)$. The output of the filter is a more continuous signal instead of a pure discrete signal, which is obtained without the filter. In this sense, the filter helps to get an average value of the voltage, taking into account past values, and the abrupt nature of the pure discrete values is smoothed, getting a better approximation for back-EMF. It is worth to be noted that the filtered voltage is only used for obtaining the back-EMF estimation. However, the filtered voltage does not necessarily decrease the bandwidth because it only affects the prediction of the back-EMF and enhances it considerably which could be observed by monitoring the T_e control signal (Fig. 9). Regarding $\vec{v}_{d,q}(k)$, it is obtaining from $\vec{v}_{\alpha,\beta}(k)$, after applying the Park's transformation. This way, $\vec{v}_{d,q_fil}(k+1)$ term will be obtained from (2) projected a sample time ahead, that is $\vec{v}_{\alpha,\beta}(k+1)$, and applying the Park's transformation and the LPF.

However, the use of the stator currents expressed in $d-q$ reference frame and filtering of stator voltage gives better results. Also, the use of a proper discretization method for the stator dynamics in the prediction of the currents (9) and back-EMF (10) has an important impact. In this sense, using the Euler discretization method for discretizing back-EMF is more adequate. Moreover, for the stator current given in the $d-q$ rotating reference frame, to obtain a more precise approximation of the load model, a second-order Taylor expansion is employed.

$$\vec{i}_{d,q}(k) = \vec{i}_{d,q}(k-1) + \frac{d\vec{i}_{d,q}}{dt}|_k\,T_s + \frac{d^2\vec{i}_{d,q}}{dt^2}|_k\,\frac{T_s^2}{2} \tag{11}$$

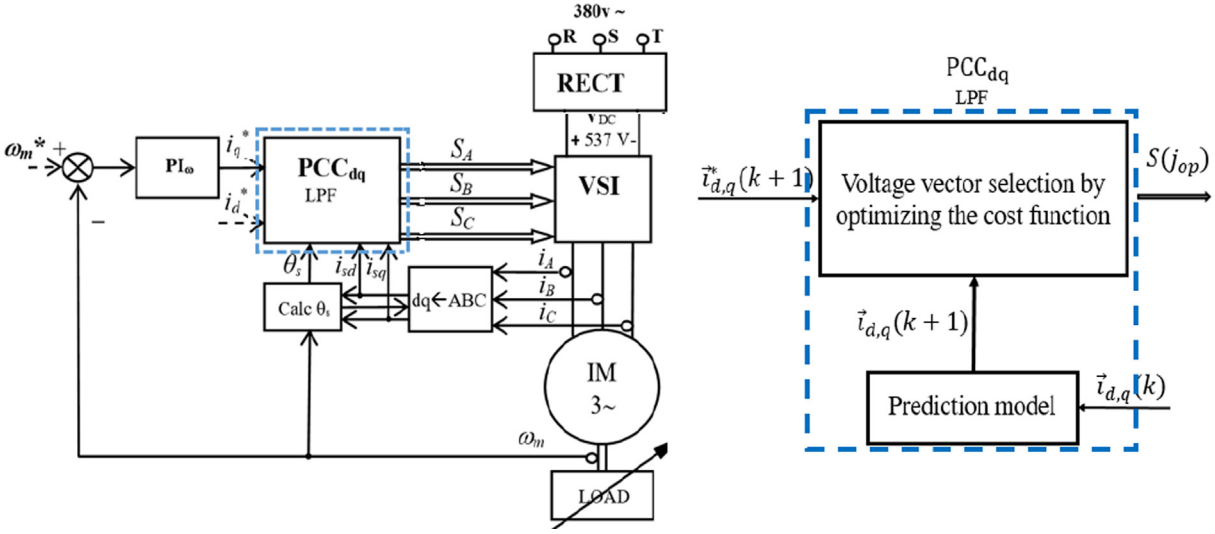

Fig. 2. Block diagram of PCC algorithm.

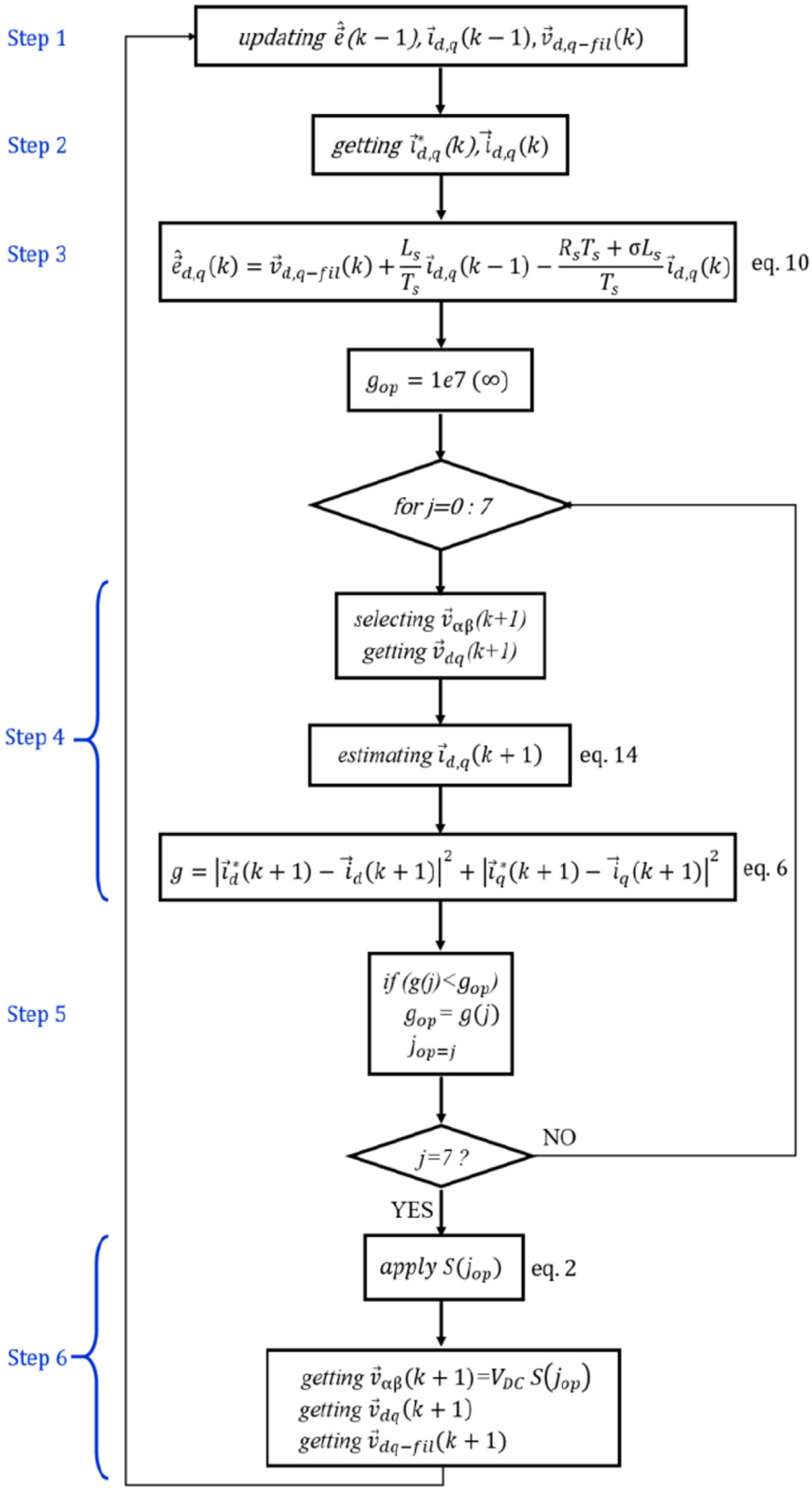

Fig. 3. Flowchart of the proposed PCC algorithm.

where considering the following approximation for the current components,

$$\frac{d\vec{i}_{d,q}(t)}{dt} \approx \frac{\vec{i}_{d,q}(k) - \vec{i}_{d,q}(k-1)}{T_s} \tag{12}$$

and,

$$\frac{d^2\vec{i}_{d,q}}{dt^2} = \frac{1}{L}\left(\frac{d\vec{v}_{d,q}}{dt} - R\frac{d\vec{i}_{d,q}}{dt} - \frac{d\vec{e}_{d,q}}{dt}\right) \tag{13}$$

and by substituting (12)and (13) in (11), and projecting it a sample period ahead, $\vec{i}_{d,q}(k+1)$ is obtained as,

$$\begin{aligned}\vec{i}_{d,q}(k+1) = {} & (-\vec{e}_{d,q}(k+1)\left(\tfrac{3T_s}{2\sigma L_s}\right) + \vec{i}_{d,q}(k) + \\ & \tfrac{T_s}{L_s\sigma}\left(\vec{v}_{d,q}(k+1) + \tfrac{\vec{v}_{d,q}(k+1) - \vec{v}_{d,q}(k)}{2}\right) + \\ & \tfrac{\vec{i}_{d,q}(k)}{2} + \tfrac{\vec{e}_{d,q}(k)}{2}\left)\left(1 + \tfrac{3T_sR}{2L_s\sigma}\right)^{-1}\right.\end{aligned} \tag{14}$$

3. Proposed PCC Method

Fig. 2 shows the blocks diagram of speed vector control of IM (based on Field Oriented Control technique), where PI_ω is the Proportional Integral speed regulator, Calc θ_s is the θ_s angle estimator, $ABC \rightarrow dq$ is the Clarke and Park transformations block, and finally, the PCC_{dq} *LPF* block is the proposed Predictive Current Controller in $d-q$ rotating reference frame with LPF. The structure of the PCC for the IM is illustrated in the Fig. 2.

One of the most important parts of PCC is the selection of the cost function to determine the optimal voltage vector. The square cost function is the error between the reference and predicted current components in $d-q$ reference frame.

The flowchart of the Fig. 3 shows the sequence of the steps that are necessary to be executed, in order to build the presented PCC algorithm. The chart can be divided in three main tasks. The first task is to get a proper estimation of the back-EMF (Step 3) with the Eq. (10), which requires the values of the previous cycle (Step 1) and the current inputs (Step 2). The second is to predict the future current of the machine (Step 4) with the Eq. (11) projected a step ahead and calculated the cost function (g) with the Eq. 6, eight times, and to select the optimal case (j_{op}), which has got the minimum value for g (Step 5). The last task is to apply the optimal voltage vector to the VSI inverter and obtain its corresponding filtered $d-q$ value (Step 6) to be used in the next cycle.

The steps of the proposed strategy are summarized as follow:

- Step 1: Updating past samples from the previous cycle: $\hat{\vec{e}}_{d,q}(k-1), \vec{i}_{d,q}(k-1)$ and $\vec{v}_{d,q-fil}(k)$.
- Step 2: Obtaining current components references from the outer regulators $\vec{i}^*_{d,q}(k)$ and measuring real current componentzs $\vec{i}_{d,q}(k)$.
- Step 3: Estimating back-EMF: $\hat{\vec{e}}_{d,q}(k)$.
- Step 4: For the 8 possible voltage vectors $j = 0:7$:
  - Selection of the voltage $\vec{v}_{\alpha,\beta}(k+1)$, applying Park transformation to get $\vec{v}_{d,q}(k+1)$ and predicting the stator current in the next sampling time: $\vec{i}_{d,q}(k+1)$.
  - Calculating the minimization function g and selecting the best (minimum) up to the actual case (j_{op}).
- Step 5: Voltage vector selection based on the minimum value of the cost function: $\vec{v}_{\alpha,\beta}(k+1)$.
- Step 6: Applying the Park transformation and LPF to the selected voltage vector ($\vec{v}_{d,q-fil}(k+1)$) for application in the next cycle.

Fig. 4. The experiment platform for IM.

Table 1
Parameters of the M2AA 132M4 ABB Induction Motor 7.5[*kW*] and 1445[*rpm*].

symbol	rated value
B_v	0.0105 [$Kgm/(rad/s)$]
J	0.0503 [Kgm^2]
L_m	0.1125 [*H*]
L_s	0.1138 [*H*]
L_r	0.1152 [*H*]
σ	0.0346
R_r	0.400 [Ω]
R_s	0.729 [Ω]
p	4 poles
$\omega_m(n)$	151.32 [rad/s](1445[*rpm*])
ϕ_r	0.9030 [*Wb*]
I_{sd}	8.026 [*A*]
I_{sq}	20 [*A*]
I_s	15.3 [*A*]
V	380 [*V*]
P_N	7500 [*W*]
μ	87%

4. Experimental validation

The proposed current regulations' performance has been validated in the MatLab/Simulink environment as well as in actual tests using a commercial IM in this section.

The control platform depicted in Fig. 4 was used to carry out the experimental validation of the proposed PCC regulator. The experimental platform is built on a commercial 7.5[*kW*] squirrel-cage IM (*M2AA*132*M*4, *ABB*) that is mechanically connected to a 10.6[*kW*] AC synchronous servo motor (190*U*2, Unimotor) on its shaft to implement the load torque(torque-controlled).

The parameters of the IM mounted in the experiment platform are listed in Table 1. Both machines are connected to a DC bus of 540[*V*] by using their respective three-phase VSI with a variety of switching frequencies. The control and monitoring tasks are done

Table 2
$THD_i(\%)$ calculation of three different discretization methods for current and back-EMF at 16.67μs (60KHz) of sampling time by using PCC_{dq-LPF}.

$\vec{i}_{d,q}$	$\vec{e}_{d,q}$ Euler	Taylor	Tustin
Euler	4.4	5	3.6
Taylor	**3.5**	3.7	5.5
Tustin	4.4	5.2	4

from a Personal Computer, which has installed the software MatLab/Simulink and dSControl, and the *DS*1103 controller board real-time interface of dSpace. An FPGA module uses measurements from an incremental encoder with 4096 impulses per revolution to compute the machine's mechanical speed.

Algorithms for speed and current control, flux and torque estimators, *theta* angle calculation, Park transformations of the reference frame, and calculations have all been implemented using a Simulink S-Function Builder block written in the *C* programming language, resulting in a compact code that is portable along different processors.

Also, The stator windings of IM have been protected by limiting the electromagnetic torque current command to 20[*A*]. The nominal value of the rotor flux (0.903[*Wb*]) is obtained by keeping the rotor flux current command at the constant value, 8.026[*A*].

Various experiments have been carried out to show the performance of the proposed method. Table 2 is presented to demonstrate the importance of the discretization method in the PCC algorithm and its impact on the value of the THD_i. Since in the PCC design process, the back-EMF and stator currents prediction need to be discretized. This table shows the value of the THD_i , by using three different discretization methods for back-EMF and currents prediction.

Moreover, the best combination, which represents the lowest THD_i after applying the LPF, has been selected to run the simulation and experiments. It is worth to be noted that before applying the filter, the best discretization method which provides the lowest THD_i in the stator current is the Euler method. This result has been obtained while the motor was working at its 100(%) rated speed (1445[*rpm*]), and the load torque was applied to the system in two steps: 10[*Nm*] at the starting point, plus 35[*Nm*] after $t = 0.7[s]$ which is 90%of rated value with a sampling time of $T_s = 16.67[\mu s]$ (60*KHz*). The lowest THD_i for stator current is achieved when back-EMF and stator current are discretized by Euler and Taylor method, respectively. Hence, the simulations and experiments are done by considering this combination, that is, the best discretization settings for back-EMF and stator currents prediction.

Fig. 5 depicts the simulation and experimental results of the performance of the machine when it is running at the 1445[*rpm*] and the sample time to execute the PCC algorithm is 12.5[μs]. The load torque is applied to the system in two steps 10[*Nm*] at the starting point, plus 35[*Nm*] after $t = 0.7[s]$. It can be noted that the simulation and the experiment test have a very similar behaviour. This makes it possible to carry out the desire tests on the simulation model in order to subsequently carry out the experiments on the real platform with the guarantee of proper system modeling. The speed tracking and accuracy are quite close to the simulation case, and it has fast dynamics. There is only a small drop in the rotor speed, and it recovers to the original reference value due to the increase in the electromagnetic torque. When it comes to the electromagnetic torque, it can be compared to its sim-

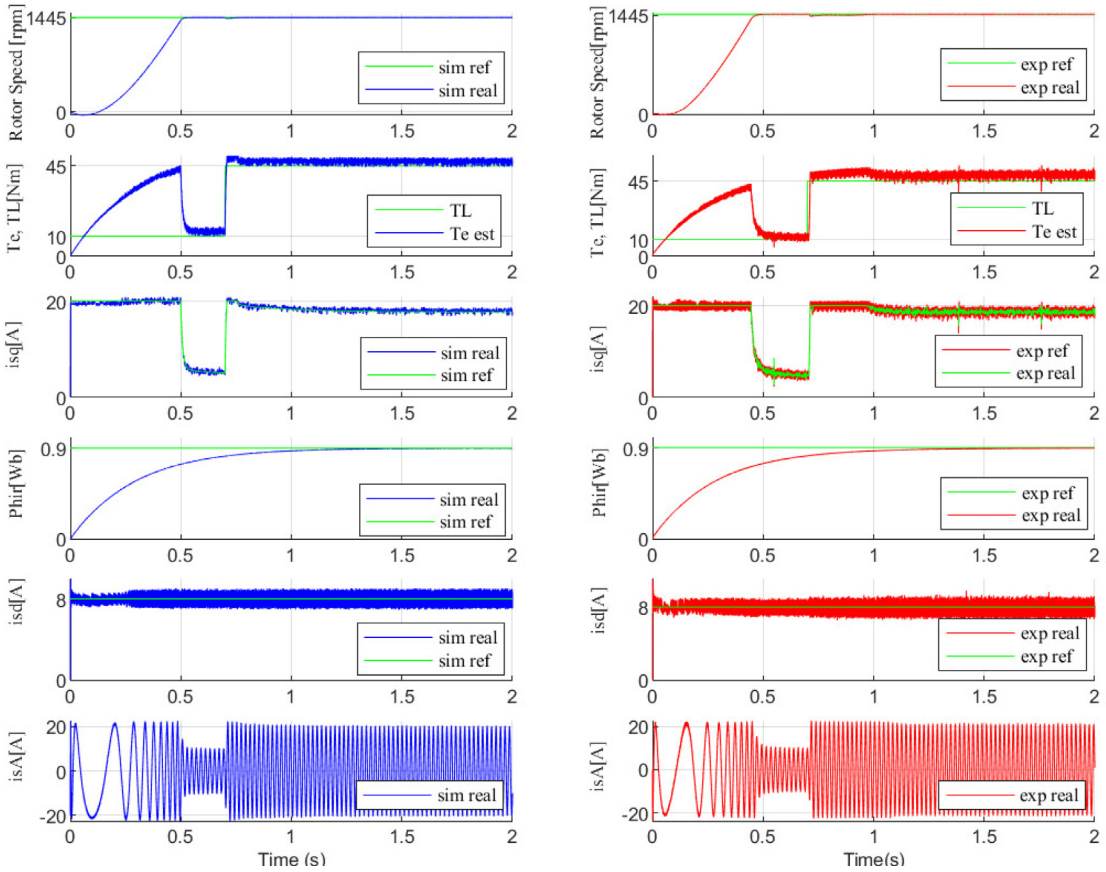

Fig. 5. Simulation and Experimental results: Dynamic response when the reference speed is 1445[*rpm*] at $T_s = 12.5[\mu s](80[KHz])$.

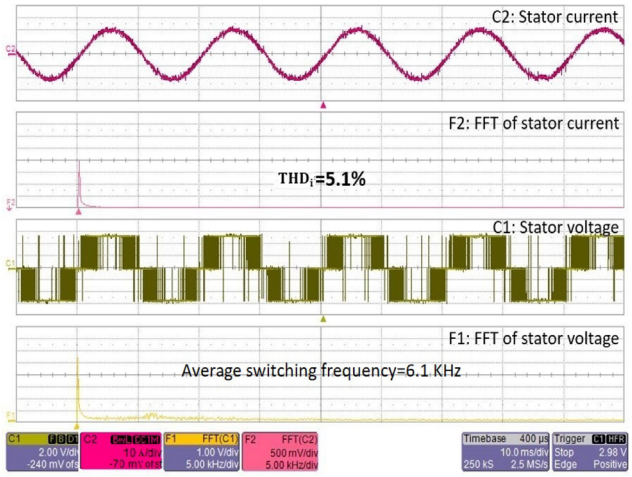

Fig. 6. Experimental results: Harmonic spectrum of stator current and voltage by using $PCC_{\alpha\beta}$, at $T_s = 12.5[\mu s](80[KHz])$.

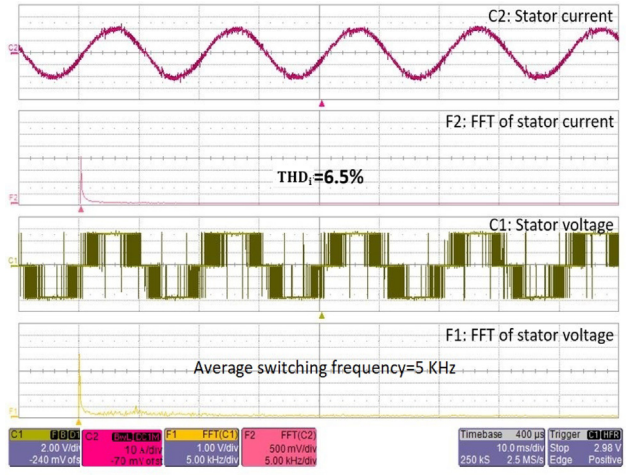

Fig. 7. Experimental results: Harmonic spectrum of stator current and voltage by using PCC_{dq}, at $T_s = 12.5[\mu s](80[KHz])$.

ulation scenario, and both are fairly comparable, smooth, and efficient. The i_{sq} torque current tracking is very satisfactory, and it is limited to its maximum value of $20[A]$. Its performance is very similar to the simulation case. The next plot illustrates the stator flux amplitude with the final of $0.9[Wb]$. This performance indicates that the stator flux is well regulated in steady state since its i_d current is efficiently controlled. Finally in the figure can be observed the low distortion of the phase A stator current and also, it is limited to $\pm 20[A]$, due to the i_q limitation. The effectiveness of the proposed PCC (PCC_{dq-LPF}) in reducing current harmonics is further confirmed by the harmonic spectrum of stator current at a steady speed of 100% of the rated value $(1445[rpm])$ and a load torque of 90% of the rated value $(45[Nm])$. The sampling time to execute the PCC algorithm is $80[KHz]$. The harmonic spectrums of current and voltage of stator are presented by applying $PCC_{\alpha\beta}, PCC_{dq}$ and PCC_{dq-LPF} methods respectively, in the Figs. 6–8. The value of the THD_i by using the proposed algorithm is 3%, which is significantly lower than others: 5.1% of $PCC_{\alpha\beta}$ and 6.5% of PCC_{dq}. It is clearly seen that the PCC_{dq-LPF} exhibit much better steady-state performance in term of current harmonics than $PCC_{\alpha\beta}$ and PCC_{dq}.

When the motor is working at the maximum rated speed and load, maximum current is needed. As a result, the switching frequency will be lower at the peak values of stator current. This observation indicates that the switching losses of the inverter will be lower. However, it is necessary to have a balance between inverter switching frequency and THD_i. By comparing Figs. 6–8, it is demonstrated that PCC_{dq-LPF} method maintains a fair balance between inverter switching frequency and THD_i. Nevertheless, $PCC_{\alpha\beta}, PCC_{dq}$ methods have lower switching losses at peak values of the stator current, but THD_i is higher.

Fig. 8. Experimental results: Harmonic spectrum of stator current and voltage by using PCC_{dq-LPF}, at $T_s = 12.5[\mu s](80[KHz])$.

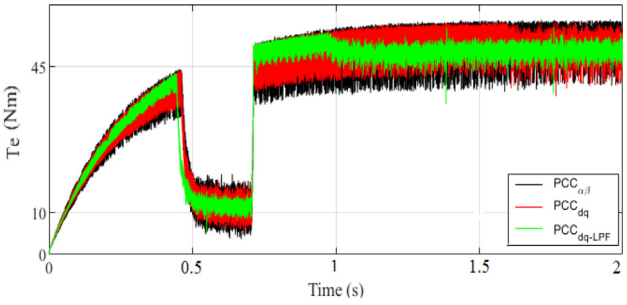

Fig. 9. Experimental results: Comparison between electromagnetic torque performance by using $PCC_{\alpha\beta}, PCC_{dq}$ and PCC_{dq-LPF}, at $T_s = 12.5[\mu s](80[KHz])$.

Fig. 9 demonstrates the efficiency of the proposed method by depicting the electromagnetic torque performance of the motor-related to the Figs. 6–8. T_e is directly related to the i_{sq} stator current. This figure makes it evident that by using the PCC_{dq-LPF}, the electromagnetic torque ripple is much lower comparing to the other two methods. This lower electromagnetic torque ripple results in less mechanical vibration of the machine and faster dynamics and response of the system is obtained, as it can be seen in the value of T_e at $0.5[s]$.

Table 3
Comparison among approaches in different ranges of the frequencies at $1445[rpm]$ and $30[Nm]$ load torque.

Sampling frequency $[KHz]$	THD_i (%) $PCC_{\alpha\beta}$	PCC_{dq-LPF}
10	25	15
40	8.4	5.8
60	7.8	5
80	7.1	4.2

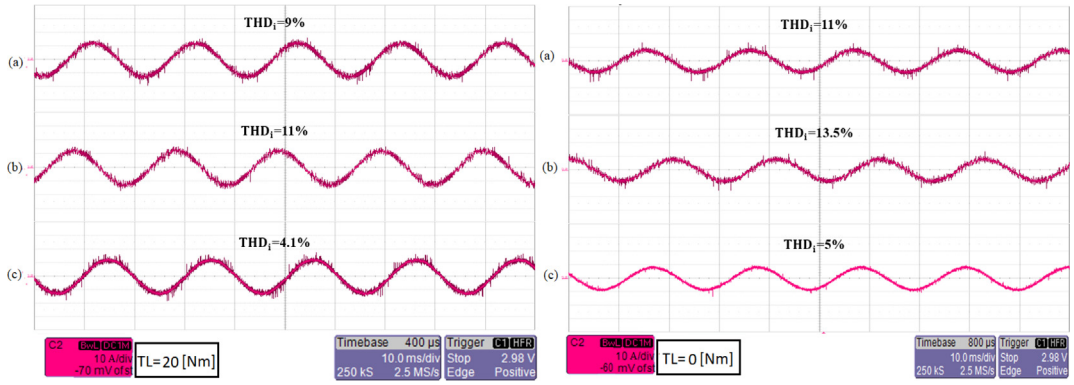

Fig. 10. Experimental results: Stator current performance at 1445[*rpm*], with a different range of torque load (TL), for (a)$PCC_{\alpha\beta}$, (b) PCC_{dq} and (c) PCC_{dq-LPF}, at $T_s = 12.5[\mu s](80[KHz])$.

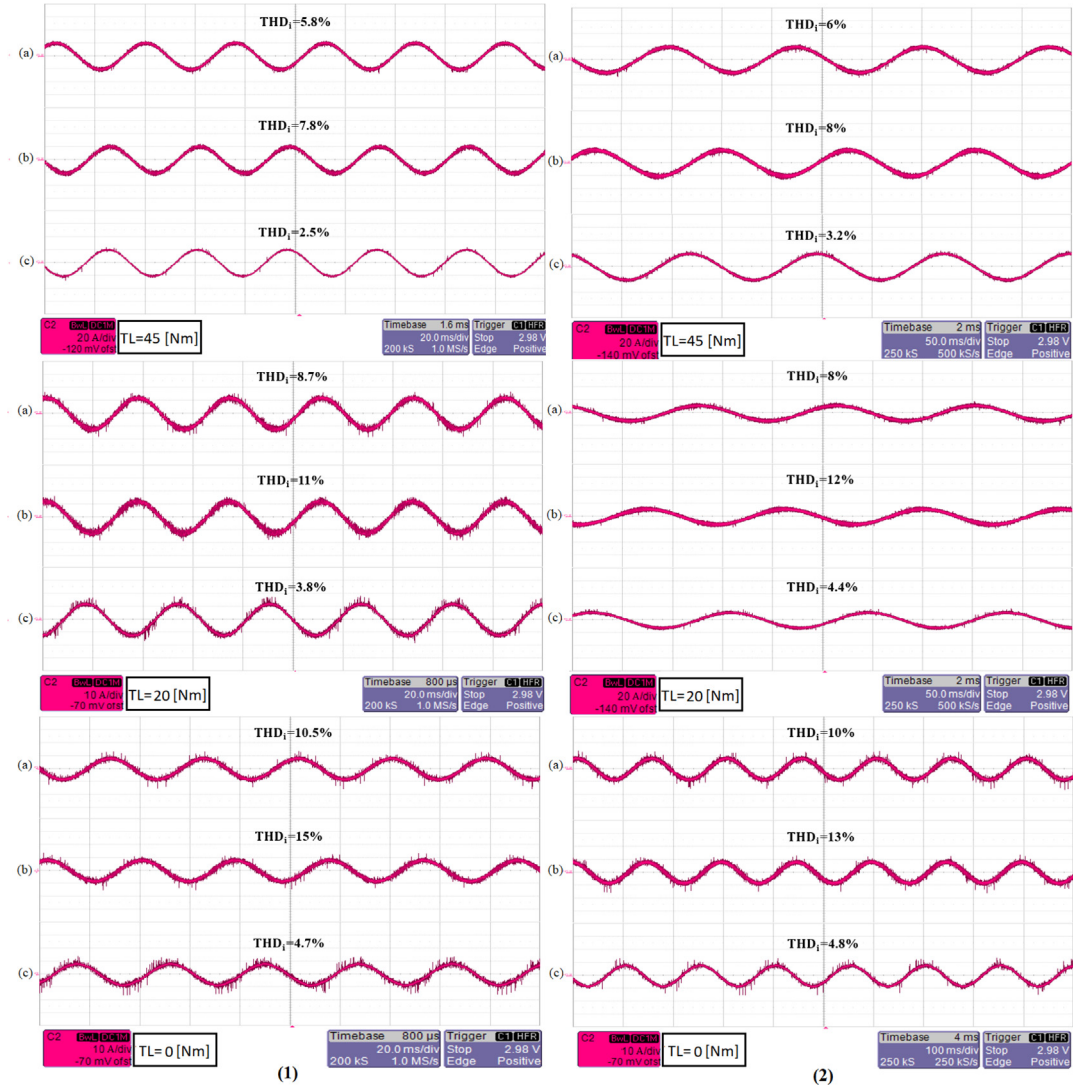

Fig. 11. Experimental results: Stator current performance at (1) 800[*rpm*] and (2) 200[*rpm*], with a different range of torque load, for (a)$PCC_{\alpha\beta}$, (b) PCC_{dq} and (c) PCC_{dq-LPF}, at $T_s = 12.5[\mu s](80[KHz])$.

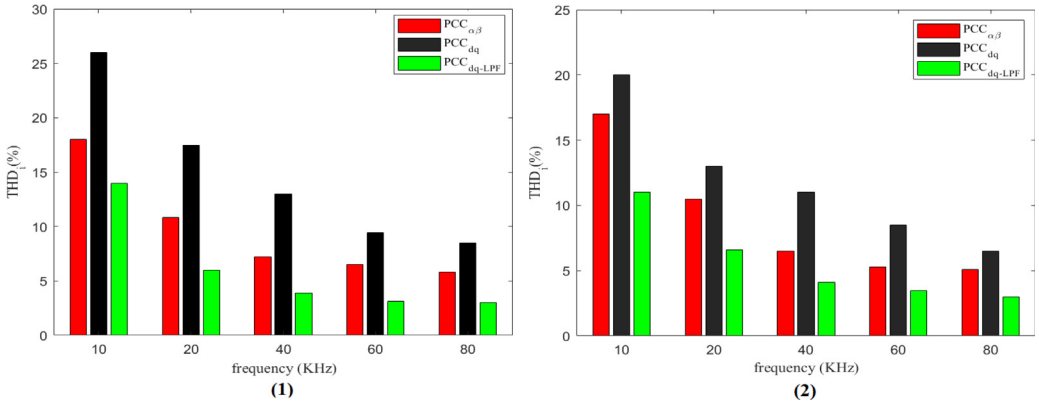

Fig. 12. Comparisons of THD_i for $PCC_{\alpha\beta}$, PCC_{dq} and PCC_{dq-LPF}, operating at (1) 1000[rpm] and (2) 1445[rpm] speed, 45[Nm] of load torque and different frequencies.

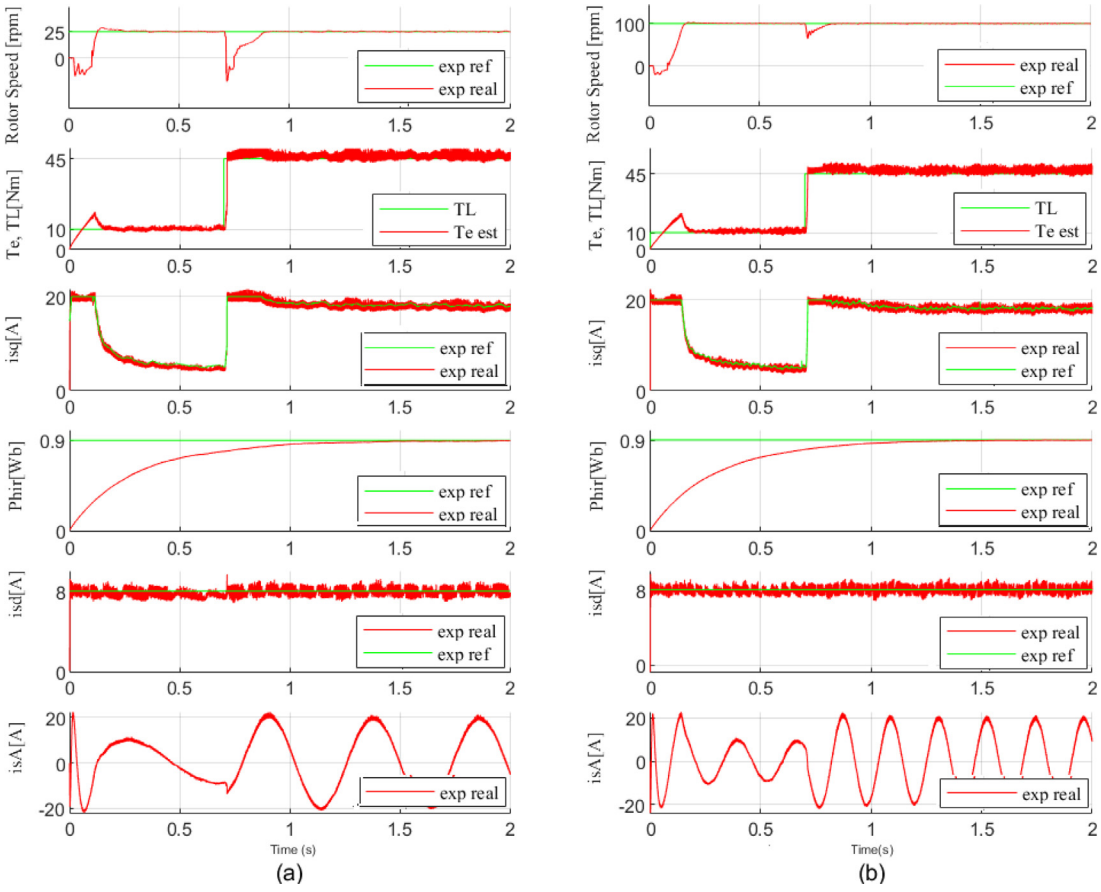

Fig. 13. Experimental results: Dynamic response at $T_s = 12.5[\mu s](80[KHz])$ when the reference speed is (a) 25[rpm] and (b) 100[rpm].

Table 3 represents the measured THD_i of stator current while IM is running at the rated speed (1445[rpm]). A load torque of 30[Nm]is applied to the machine at $t = 0.7[s]$. As in the previous experiments, stator current has less distortion by using PCC_{dq-LPF} controller.

Fig. 10 and Fig. 11 are presented to illustrate the performance of the propose controller in wide range of speed and torque load. Based on the results, it is evident that by decreasing the load torque, THD_i increases. However, it is notable that PCC_{dq-LPF} performs a better behaviour compare to $PCC_{\alpha\beta}$ and PCC_{dq} methods.

Fig. 12 provides the numerical comparisons of current THD_i for different PCC methods at various frequencies while IM is running at two different speeds. As it can be extracted, as the sampling frequency of the controller is increasing, current THD_i is decreasing. However, by comparing the values of THD_i in rotating reference frame and stationary reference frame, it is evident that, by using proposed PCC_{dq-LPF}, the distortion factor of current reduces significantly.

It is worth mentioning that use of LPF has its drawbacks; specifically the performance of the filter at low operating speed due to the sensitivity for the corner frequency change. In this regard, the following experiments are carried out to discover the range of speed that the proper performance of machine could be guaranteed while applying the proposed method. Based on the performed

Table 4
THD_i (%) calculation, using PCC_{dq-LPF} method in a range of low speed and different load torque at $T_s = 12.5[\mu s](80[KHz])$.

Speed [rpm]	THD_i (%) $TL = 0$	$TL = 20[Nm]$	$TL = 45[Nm]$
100	5	4.3	3.3
50	5.5	4.4	3.2
25	6	3.8	3

experiments, It turns out this proposal guarantees a proper performance for the experimental platform in a range of motor speed from $25[rpm]$ to the rated speed which is $1445[rpm]$.

Fig. 13 depicts the dynamic performance of the IM when machine is rotating at $25[rpm]$ and $100[rpm]$. The applied load torque is $45[Nm]$ and the sampling time of the PCC algorithm execution is $80[KHz]$. As it is indicated, the rotor speed, T_e, d and q stator current components and stator phase current have an appropriate performance in both mentioned velocities.

Also, Table 4 demonstrates the THD_i measurement when motor is working in a range of low speed with different load torque conditions. As reflected, in low speed the PCC_{dq-LPF} can oath a suitable stator current ripple percentage.

5. Conclusion

An enhanced PCC regulator was developed and implemented for IM drives: PCC_{dq-LPF}. The proposed algorithm is designed in the $d-q$ rotating reference frame and it includes an LPF to improve the THD_i and the electromagnetic torque ripple in compared to the conventional methods. Furthermore, a Taylor series expansion is used for the discretization of the IM model, which leads to a good balance between model accuracy and complexity. The main advantages of this proposal are simplicity of implementation and low computational burden. The effectiveness of the proposed controller has been validated in the various experimental test conditions. The PCC_{dq-LPF}model has been compared with the $PCC_{\alpha\beta}$ and PCC_{dq} approaches. The experimental analysis demonstrates that the proposed $PCC_{dq}(PCC_{dq-LPF})$ is more effective than the other two approaches, getting drastic reduction of THD_i and electromagnetic torque ripple. THD_i diminution: $34\% - 41\%$ respect to the $PCC_{\alpha\beta}$ and $45\% - 62\%$ respect to the PCC_{dq}, and T_e ripple lowering: 40% respect to the $PCC_{\alpha\beta}$ and 50% respect to the PCC_{dq}. All in all, considering the importance of the low THD_i in power systems, PCC_{dq-LPF} can be implemented in industrial applications in a wide range of speed $(25[rpm] - 1445[rpm])$ to achieve a desire THD_i which is compatible with international standards such as $IEC61000-3-2$ and $IEEE519$ since it is easy to implement and also does not imply a high computational cost.

Financial Disclosure

The University of the Basque Country (UPV/EHU) [Grant No. PIF 18/127] has funded the research in this paper.

Conflict of Interest

None reported.

Acknowledgments

The authors wish to express their gratitude to the Gipuzkoako Foru Aldundia through the project Etorkizuna Eraikiz 2022–2023, the Basque Government through the project EKOHEGAZ (ELKARTEK KK-2021/00092), the Diputacion Foral de Alava (DFA) through the project CONAVANTER, and to the UPV/EHU through the project GIU20/063 for supporting this work.

References

[1] Camacho EF, Alba CB. Model predictive control. Springer science & business media; 2013.
[2] Pervez M, Kamal T, Fernández-Ramírez LM. A novel switched model predictive control of wind turbines using artificial neural network-markov chains prediction with load mitigation. Ain Shams Engineering Journal 2022;13(2):101577.
[3] Shiravani F, Cortajarena JA, Alkorta P, Barambones O. Generalized predictive control scheme for a wind turbine system. Sustainability 2022;14(14).
[4] Li H, Chen S. A neural-network-based model predictive control scheme for grain dryers. Drying Technology 2019.
[5] Kassem AM. Neural predictive controller of a two-area load frequency control for interconnected power system. Ain Shams Engineering Journal 2010;1(1):49–58.
[6] Sultana WR, Sahoo SK, Saikiran KS, Reddy GR, Reddy PH. A computationally efficient finite state model predictive control for cascaded multilevel inverter. Ain Shams Engineering Journal 2016;7(2):567–78.
[7] Taher Ahmed M, Hasanien Hany M, Ginidi Ahmed R, Taha Adel TM. Hierarchical model predictive control for performance enhancement of autonomous microgrids. Ain Shams Engineering Journal 2021;12(2):1867–81.
[8] Yang N, Li D, Zhang J, Xi Y. Model predictive controller design and implementation on fpga with application to motor servo system. Control Engineering Practice 2012;20(11):1229–35.
[9] Carron A, Arcari E, Wermelinger M, Hewing L, Hutter M, Zeilinger MN. Data-driven model predictive control for trajectory tracking with a robotic arm. IEEE Robotics and Automation Letters 2019;4(4):3758–65.
[10] Wang J, Wang F, Wang G, Li S, Yu L. Generalized proportional integral observer based robust finite control set predictive current control for induction motor systems with time-varying disturbances. IEEE Transactions on Industrial Informatics 2018;14(9):4159–68.
[11] Bekakra Youcef, Zellouma Laid, Malik Om. Improved predictive direct power control of shunt active power filter using GWO and ALO–Simulation and experimental study. Ain Shams Engineering Journal 2021;12(4):3859–77.
[12] Jonnala Rohith Balaji, Sai Babu, Ch. A modified multiband hysteresis controlled DTC of induction machine with 27-level asymmetrical CHB-MLI with NVC modulation. Ain Shams Engineering Journal 2018;9(1):15–29.
[13] Shiravani Fahimeh, Alkorta Patxi, Cortajarena Jose Antonio, Barambones Oscar. An Integral Sliding Mode Stator Current Control for Industrial Induction Motor. Mathematics 2022;10(15):2765.
[14] Areed Fayez G, Haikal Amira Y, Mohammed Reham H. Adaptive neuro-fuzzy control of an induction motor. Ain Shams Engineering Journal 2010;1(1):71–8.
[15] Z. Yi, A.J. Babqi, Y. Wang, D. Shi, A.H. Etemadi, Z. Wang, B. Huang, Finite-control-set model predictive control (fcs-mpc) for islanded hybrid microgrids, in: 2018 IEEE Power & Energy Society General Meeting (PESGM), IEEE, 2018, pp. 1–5.
[16] Rodriguez J, Pontt J, Silva CA, Correa P, Lezana P, Cortés P, Ammann U. Predictive current control of a voltage source inverter. IEEE transactions on industrial electronics 2007;54(1):495–503.
[17] Vazquez S, Rodriguez J, Rivera M, Franquelo LG, Norambuena M. Model predictive control for power converters and drives: Advances and trends. IEEE Transactions on Industrial Electronics 2016;64(2):935–47.
[18] S.P. Pimentel, O. Husev, D. Vinnikov, C. Roncero-Clemente, S. Stepenko, An indirect model predictive current control (ccs-mpc) for grid-connected single-phase three-level npc quasi-z-source pv inverter, in: 2018 IEEE 59th International Scientific Conference on Power and Electrical Engineering of Riga Technical University (RTUCON), IEEE, 2018, pp. 1–6.
[19] A. Alkasir, S.E. Abdollahi, S.R. Abdollahi, P. Wheeler, A primary side ccs-mpc controller for constant current/voltage charging operation of series-series compensated wireless power transfer systems, in: 2021 12th Power Electronics, Drive Systems, and Technologies Conference (PEDSTC), IEEE, 2021, pp. 1–5.
[20] İ. Şahin, O. Keysan, A simplified discrete-time implementation of fcs-mpc applied to an im drive, in: 2019 21st European Conference on Power Electronics and Applications (EPE'19 ECCE Europe), IEEE, 2019, pp. P–1.
[21] Li H, Liu Y, Yang J. A novel fcs-mpc method of multi-level apf is proposed to improve the power quality in renewable energy generation connected to the grid. Sustainability 2021;13(8):4094.
[22] A. Tian, C. Gao, J. Lv, X. Jiang, Ccs-mpc for pmsm with wide speed range based on variable dc-bus voltage control applied to the flywheel energy storage system, in: E3S Web of Conferences, Vol. 271, EDP Sciences, 2021.
[23] Garcia C, Rodriguez J, Silva C, Rojas C, Zanchetta P, Abu-Rub H. Full predictive cascaded speed and current control of an induction machine. IEEE Transactions on Energy Conversion 2016;31(3):1059–67.
[24] Zhang Y, Xia B, Yang H, Rodriguez J. Overview of model predictive control for induction motor drives. Chinese Journal of Electrical Engineering 2016;2(1):62–76. doi: https://doi.org/10.23919/CJEE.2016.7933116.
[25] Martinez JLR, Arashloo RS, Salehifar M, Moreno JM. Predictive current control of outer-rotor five-phase bldc generators applicable for off-shore wind power plants. Electric Power Systems Research 2015;121:260–9.
[26] Morel F, Lin-Shi X, Retif J-M, Allard B. A predictive current control applied to a permanent magnet synchronous machine, comparison with a classical direct torque control. Electric Power Systems Research 2008;78(8):1437–47.
[27] Ishaq M, Che Y, Ullah K. Switching regulation in the control of 5-phase permanent magnet synchronous motor fed by 3×5 direct matrix converter. European Journal of Electrical Engineering 2021;23(1):27–35.

[28] Silva CA, Yuz JI. On sampled-data models for model predictive control. In: IECON 2010–36th Annual Conference on IEEE Industrial Electronics Society. IEEE; 2010. p. 2966–71.
[29] Rojas CA, Yuz JI, Aguirre M, Rodriguez J. A comparison of discrete-time models for model predictive control of induction motor drives. In: in: 2015 IEEE International Conference on Industrial Technology (ICIT). IEEE; 2015. p. 568–73.
[30] P. Vaclavek, P. Blaha, Pmsm model discretization for modelp predictive control algorithms, in: Proceedings of the 2013 IEEE/SICE International Symposium on System Integration, IEEE, 2013, pp. 13–18.
[31] Li J, Huang X, Niu F, You C, Wu L, Fang Y. Prediction error analysis of finite-control-set model predictive current control for ipmsms. Energies 2018;11 (8):2051.

Fahimeh Shiravani received the B.S. degree in Electrical engineering from Jundi-shapur University of Technology, Dezful, Iran, in 2014 and the M.S. degree in Electrical Engineering (specialty Control Engineering), in 2016, from Shiraz University of Technology, Faculty of Electrical and Electronic Engineering, Shiraz, Iran. She is currently perusing the Ph.D. degree in Control, Automation, and Robotic at the University of the Basque Country, Eibar, Spain. Her main research interests are nonlinear control theories, robust control methods, and electrical machine drives.

Patxi Alkorta received the Engineer in Electronics (specialty Automatic Control), in 2004, from the University of the Basque Country (UPV/EHU), Faculty of Science and Technology of Leioa, Spain. He received the Ph. D in Robotics and Automatic Control Systems from UPV/EHU in 2011. He teaches in the Systems Engineering and Automatics Department from the School of Engineering of Eibar (UPV/EHU). His main research interests are the induction motor drives; speed and position control, variable structure control and predictive control.

José Antonio Cortajarena received the Engineer in Electronics (specialty Automatic Control), in 2003, from the University of the Basque Country (UPV/EHU), Faculty of Science and Technology of Leioa, Spain. He is teaching in the Electronic Technology Department from the School of Engineering of Eibar (UPV/EHU). His main research interests are the electric machines: torque, speed and position control; sensorless control and intelligent control. Also, renewable energy and grid connection and control are of his interest.

Oscar Barambones received the M. Sc. degree in applied Physics (specialty Electronics and Automatic Control) and the Ph. D degree, both from the University of the Basque Country (UPV/EHU), Faculty of Science and Technology of Leioa, Spain in 1996 and 2000, respectively. He teaches in the Systems Engineering and Automatics Department from the School of Engineering of Vitoria (UPV/EHU). His main research interests are the induction machine drives; speed control, position control, variable structure control and predictive control.